Molecular Dynamics Simulations

Multi-component Amorphous Glasses: Effect of Glass Compositions

Pooja Sahu[1,2], *Sk. Musharaf Ali[1,2], K.T. Shenoy[1], A. Arvind[3], G. Sugilal[3], C.P. Kaushik[3]

[1]Chemical Engineering Division, Bhabha Atomic Research Centre, Mumbai-400085, India

[2]Homi Bhabha National Institute,Mumbai-400094, India

[3]Nuclear Recycle Group, Bhabha Atomic Research Centre, Mumbai-400085, India

ABSTRACT

Selection of suitable glass composition for vitrification of high-level radioactive waste (HLWs) is one of the major challenges in nuclear waste reprocessing. Atomic and molecular level understanding can help in preliminary screening and thus reduce the dependency to some extent on tedious experimental procedures. In that context, extensive molecular dynamics (MD) have been carried out, which provides microscopic understanding of the glass structure and phenomena associated with the change in glass compositions. A detailed view of local structure and medium range connectivity has been explored. Results showed a good match of evaluated macroscopic glass parameters: density (ρ), glass transition temperature (T_g) and thermal expansion coefficient (TEC) with the experiments. The presented results might be of great scientific use for future glasses in various applications including nuclear waste immobilization.

Keywords: Sodium Borosilicate Glass, Molecular Dynamics Simulation, Glass Transition Temperature, Bridging Oxygen, Structure Factor, Diffusion, Chemical Durability.

Introduction

Glass is an amorphous solid with a wide spectrum of applications in electronic display and devices, cover glasses and other valuable domestic/laboratory wares[1]. The popularity of borosilicate glasses in nuclear waste immobilization[2,3] arises due to a combination of useful material properties including high chemical durability, resistance to crystallization/devitrification and the ability to accommodate a wide diversity of cations within its structure. In addition, borosilicate glasses can be produced in large quantities in remotely handled plant environments owing to the maturity of glass production technology. Each individual component of glass plays a significant role in deciding the glass property and strength[4]. Even a minor change in composition might lead to a substantial difference in glass properties. Basic understanding about the macroscopic properties of the glasses is pursued after the microscopic structure at the atomic/molecular level. Earlier Boron-11 NMR has been widely applied to study the structure of borosilicate glasses[5-7]. Besides NMR, high temperature Raman scattering spectroscopy has also been used by Osipov *et al.*[8] to examine the stability of amorphous nature in glass and melts. A significant contribution has been made by Yang *et al.*[9] in identifying the structure and dissolution properties of boro-phospho-silicate glasses using Solid-State NMR as well as molecular dynamics (MD) Simulations[10,11]. Constituents such as silica and boric oxide are the major network formers. In addition to the role of network formers, the physical properties of vitrified glass are also known to have clear dependence on the nature and quantity of the added alkali modifiers. In particular, the dependence on the nature of alkali modifiers originates from structural variation. Though numerous experimental as well as simulation studies report the dependence of glass properties on the nature and quantity of the added alkali modifiers, however, studies by Stevensson *et al.*[12] showed that the effects introduced by the nature of alkali oxides are negligible. Such disagreements drive the further research on the glass structure and properties with varied compositions. Though severe structural changes in B-bearing glasses has been observed with variation in composition, temperature or pressure, however, despite of popularity, the long long-lasting challenges of microscopic structural evidence are yet to be explored for these glasses. In contradiction to 'Loewenstein avoidance rule', Yu *et al.*[13] showed the abundant presence of BO_4-BO_4 motifs in alkali/alkaline-earth borosilicate glasses. The relative propensity of finding P-O-Q (where P /and/or Q = Si, B3, and B4; where B3 and B4 respectively represent the BO_3 trigonal structural units and BO_4- tetrahedral structural units of boron) links was observed to be composition dependent. Surprisingly, for few composition of glasses, especially with B4 fraction higher than 0.6, relative propensity of B4-O-B4 linking was higher than B3-O-B3, which contracts the general thought of 'B[4] avoidance rule' as predicted by many theories[14,15], hereby, demand for furthermore studies. Besides the experimental and MD studies, numerous efforts were made by many theoretical models established by Phillips *et al.*[16], Williams and Scott *et al.*[17], Soga *et al.*[18], and Bridge *et al.*[19] in this direction. However, most of these models consider only first neighbour influence and therefore are restricted to find the structural changes within certain limits only.

Considering all this, the present study is dedicated to understand the short-range order and medium range connectivity of borosilicate glasses. The correlations between microscopic structure and macroscopic glass properties such as glass transition temperature, thermal expansion coefficient and mechanical integrity has been established. In addition, the diffusion dynamics of component species has been determined, which can be utilized to demonstrate the long-term leaching ability and radiation stability of these glasses. The MD results provide the reasoning for the relative

order of observed macroscopic properties from microscopic point of view. A detailed view of local structure and medium range connectivity has been explored.

Computational methods

The present simulations were conducted with LAMMPS package[20]. The interaction between atoms was simulated using the combination of Buckingham potential (for short-range interactions and Coulomb potential (for long-range interactions, expression, together known as Van Beest, Kramer, Van Santen (BKS) potential model[21].

$$U_{vdw} = \sum_{i=1}^{N}\sum_{j>i}^{N} A_{ij} e^{-r_{ij}/\rho_{ij}} - \frac{C_{ij}}{r_{ij}^{6}} \quad (1)$$

$$U_{coul} = \frac{q_i q_j}{4\pi\varepsilon r_{ij}} \quad (2)$$

The parameters ρ_{ij}, A_{ij} and C_{ij} control the narrowness of potential model. The separation between the i^{th} and j^{th} atom, having partial charge q_i and q_j respectively is represented by r_{ij} and ε is the permittivity. The forcefield parameters of simulated glasses can be found in our previous papers[22,23].

Particle-Particle-Particle Mesh (PPPM) method[24] was employed to account for the long-range interactions. The partial charge on the atoms were taken to be composition dependent[25]. All systems were initially heated at 5000 K using the canonical (NVT) ensemble for 10 ns in order to remove the memory effects. This was followed by NVT quenching at a rate of 0.4 K/ps. The systems were furthermore equilibrated for 20 ns dynamics using the isothermal- isobaric ensemble (NPT)[26] at 300 K and P = 1 atm. Further, the production runs were performed for 30 ns, and the generated data was utilized for the analysis of structural and dynamical properties of simulated glass, with methods as discussed in our previous articles[22,23].

Results and discussion

Pure Glass Matrix of SiO_2 and B_2O_3

First, the pure glass matrix of major network formers: SiO_2 and B_2O_3 were simulated, images shown in Fig.1(a). The density was measured to be 2.38 g/cm^3 for SiO_2 and 1.82 g/cm^3 for B_2O_3, which is close to respective experimental densities. The radial distribution function (RDF) showed the peak positions at 1.62 Å, 2.58 Å and 3.17 Å respectively for Si-O, O-O and Si-Si in SiO_2 and at 1.35 Å, 2.37Å and 2.57 Å corresponding to B-O, O-O and B-B in B_2O_3.

The coordination number, and bond/angle distributions are shown in Fig.1(b, c). In sequence, the structure factor in Fig.1(d) was estimated in order to determine the intermediate range order in these glasses. SiO_2 showed the first peak at ~2.15-2.25 Å^{-1} and then a second peak at around 5.45 Å^{-1}, while, B_2O_3 showed first peak at 2.4-2.45 Å^{-1} and a negative dip at 3.0 Å^{-1}. The first sharp diffraction peak (FSDP) was noted at 1.2-1.3 Å^{-1} for two connected SiO_4 tetrahedrals and at 1.45-1.65 Å^{-1} for two connected trigonal boron (BO_3) units.

Furthermore, the characteristic vibration spectrum VDOS of SiO_2 shows a flat peak at 200-600 cm^{-1}, and another peak in between ~1050-1070 cm^{-1} concerning intra-tetrahedral excitations. VDOS spectrum of B_2O_3 shows four characteristic peaks at 130 cm^{-1}, 670 cm^{-1}, 960 cm^{-1} and 1180 cm^{-1} (Fig.1(e)). The first two peaks are related to vibration of B atoms[27], while higher peaks represent the vibration of oxygen atoms connected to trigonal coordinated boron. Essentially, the selected potential parameters well reproduce the experimental VDOS and earlier reported data[27,28].

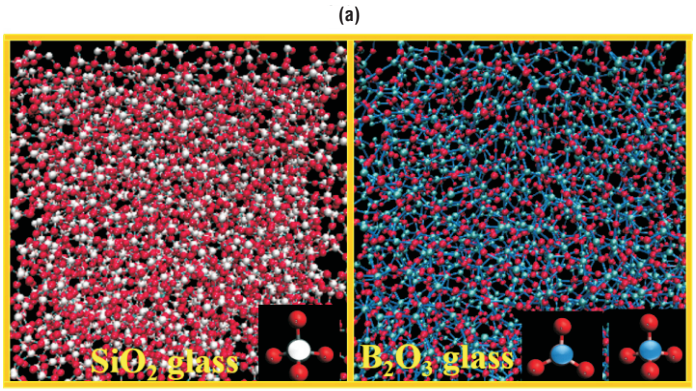

Fig.1(a): Snapshot for structure of amorphous SiO_2 and amorphous B_2O_3 (Color code: Si: white, O: red, B: blue) Inset images shows SiO_4 tetrahedra, BO_3 planer structure and BO_4- tetrahedral unit.

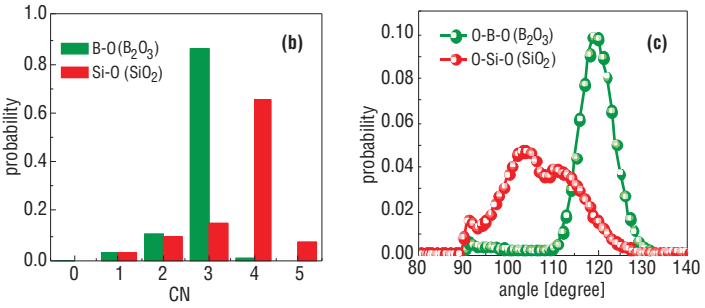

Fig.1(b): coordination distribution profile and **(c)** angle distribution profile for SiO_2 and B_2O_3 glass.

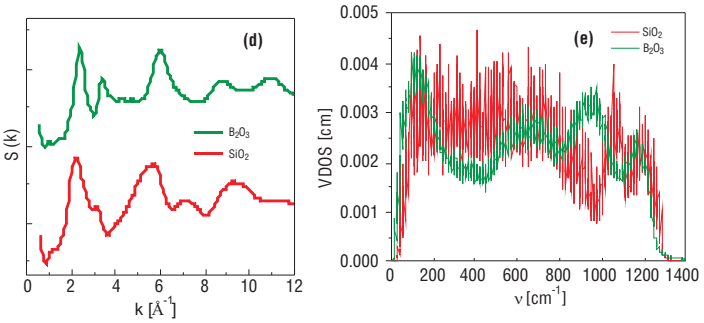

Fig.1(d): Total structure factor and **(e)** vibration density of state (VDOS) for SiO_2 and B_2O_3.

Binary borosilicate glass

The structural models of borosilicate glass were prepared using different composition of SiO_2 and B_2O_3 in the matrix. The results in Fig.2(a) show that the density of glass was increased from 1.75 g/cm^3 to 2.14 g/cm^3, while increase in SiO_2 concentration from 10% to 70%. Also, it was noticed from Fig.2(b) that the increase in silica content leads to increased conversion of planer BO_3 (B3) units into BO_4- (B4) tetrahedrals. In particular, the network connection becomes stronger with higher concentration of SiO_2 in the glass matrix.

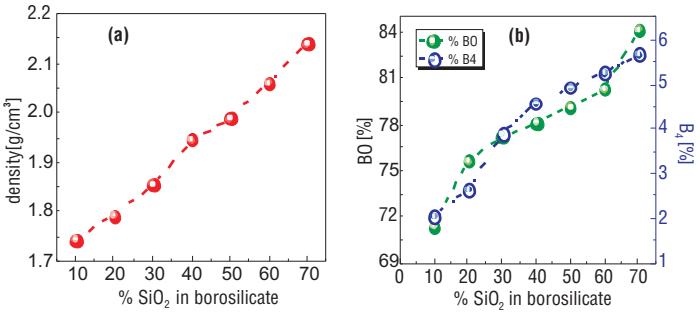

Fig.2(a): density and **(b)** bridging oxygen atoms (BO) (left Y axis) and BO_4- (B4) units (right Y axis) in borosilicate glass matrix.

Effect of Alkali addition: sodium silicate & sodium borate

The BOs were reduced with increasing Na_2O content (Fig.3(a)), which reflect that the excess alkali may lead to devitrification of glass and therefore need to be avoided. The density of sodium borate was seen to be increasing with the increase in Na_2O concentration till 40%, thereafter a decrease in density was observed with further addition of Na_2O as shown in Fig.3(b). In precise, the initially added sodium ions (for Na_2O < 40%) were seen to reside within the cavities formed by boroxyl rings, on the contrary, furthermore added sodium ions were observed to participate as network modifier. Occupancy of sodium ions in the interstitial positions causes larger increase in mass than the volume of glass matrix, therefore leads to increasing density with Na_2O concentration smaller than 40%. At the same time, the presence of alkali ions within the boroxyl cavities provides the charge compensation to BO_4- tetrahedrals and so contribute in $BO_3 \rightarrow BO_4$- conversion. As a results, the fraction of B4 in sodium borate glass matrix was observed to be increased with increase in Na_2O for concentration smaller than 40%. Such an altering behaviour of sodium ions in sodium borate glass was also confirmed by the angle distribution profiles shown in Fig.3(c). Akin to sodium silicate matrix, the BOs were reduced with increase in alkali concentration in the sodium-borate glass as shown in Fig.3(d).

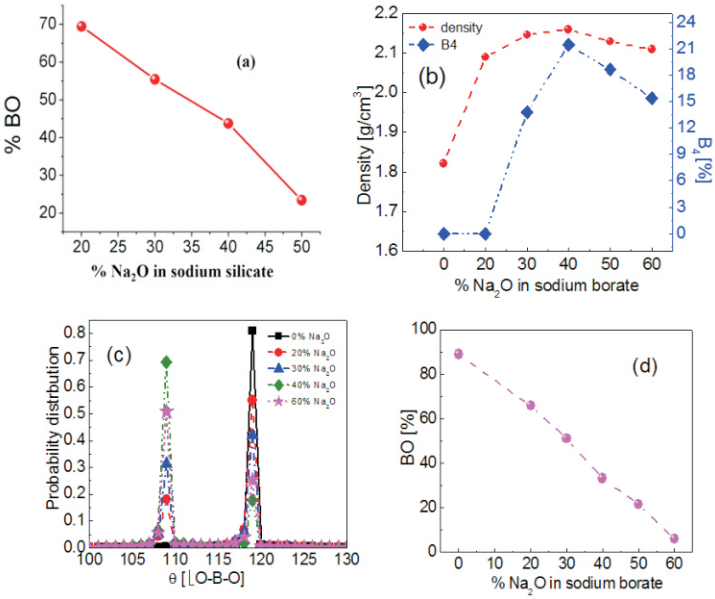

Fig.3(a): Number of BO in sodium silicate glass **(b)** density (left Y axis) and B4 units (right Y axis) in sodium borate glass matrix, **(c)** angle distribution profile for O-B-O in sodium borate glass matrix and **(d)** number of BO in sodium borate glass matrix.

Sodium borosilicate glass matrix (NBS)

Furthermore, the NBS glass with composition $21SiO_2.6B_2O_3.7Na_2O$ i.e. 59.70% SiO_2, 19.76% B_2O_3 and 20.53 %Na_2O was simulated, structure shown in Fig.4 (a). The density was measured to be 2.42 g/cm^3, which was in good agreement with the experimental density (*2.4 g/cm^3). The coordination and angle distribution profiles are shown in Fig.4(b, c) respectively. The CN was measured to be 4.0, 3.8 and 10.28 for Si-O, B-O and Na-O respectively. Also, the angle distribution profiles show tetrahedral coordination of oxygen to Si as peak for O-Si-O was obtained at 109.4°. Two peaks were noticed for O-B-O at 109.4° as well as at 120°, indicating tetrahedral coordination and trigonal coordination of B with O. The relative concentration of BO_4- and BO_3 was estimated to be ~63% and 29% respectively. The peaks for angles Si-O-Si, B-O-B and O-Na-O were found to be rather broad in nature, with peak position of 146°, 138° and 151° respectively, which is in good agreement with the available data[29].

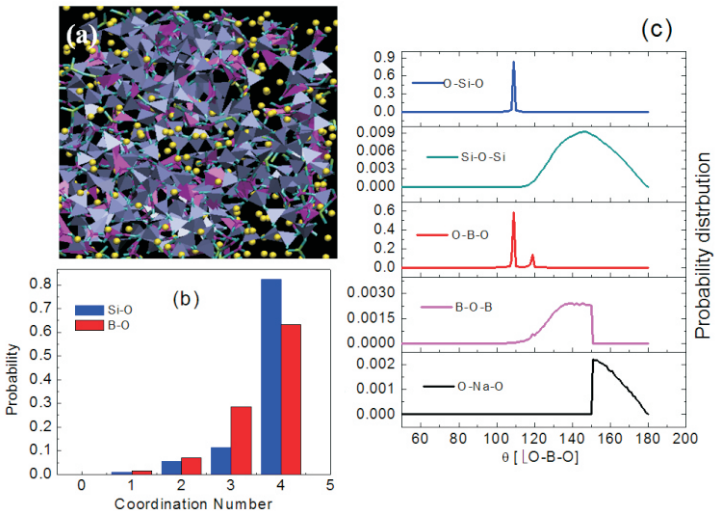

Fig.4(a): Snapshot for sodium borosilicate glass matrix [SiO_4 tetrahedrals shown blue, BO_3 & BO_4- units purple and sodium ions are shown yellow] **(b)** coordination number distribution and **(c)** angle distribution in sodium borosilicate (NBS) glass matrix.

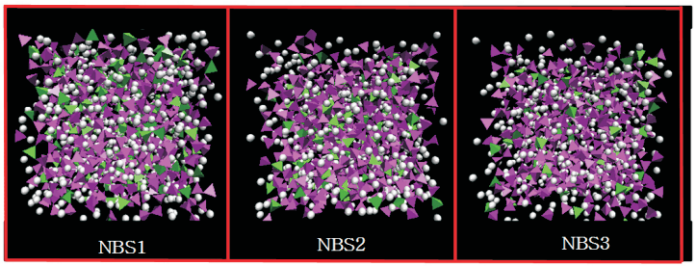

Fig.5: Snapshot for sodium borosilicate glass matrix SiO_4 tetrahedrals shown purple, BO_3 & BO_4- units green.

Table 1. Composition of NBS glasses

	N_{SiO_2}	$N_{B_2O_3}$	N_{Na_2O}	N_{total}
NBS1	720	262	328	4454
NBS2	780	260	260	4420
NBS3	700	350	260	4630

Subsequently, the composition dependence was tested by simulating three compositions of NBS glass matrix, named as NBS1, NBS2, and NBS3, composition shown in Table 1 and respective snapshots in Fig.5.

Table 2. Density, Number of Bridging Oxygens (BO), Non-Bridging Oxygen (NBO) and BO_4- (B4) fraction in simulated NBS glasses.

	Density [$g.cm^{-3}$]	% BO	% NBO	% B4
NBS1	2.273	80.23	19.77	57.44
NBS2	2.275	83.77	16.23	58.26
NBS3	2.269	82.43	17.57	48.42

Table 3. RDF First Peak Positions (r_{max}) and Coordination Number (CN) for sodium borosilicate glasses.

Pair	NBS1		NBS2		NBS3	
	r_{max}	CN	r_{max}	CN	r_{max}	CN
Si-O	1.61	4.00	1.61	4.00	1.61	4.0 0
B-O	1.62	3.67	1.54	3.63	1.62	3.56
Na-O	2.5	5.67	2.49	5.54	2.5	6.00
Si-Si	3.19	1.77	3.15	2.03	3.21	1.15
Si-B	3.09	1.94	3.09	1.82	3.13	2.81
B-B	3.05	1.22	3.03	1.23	3.14	1.47

The results in Table.2 show that the NBS2 had higher density than NBS1, as R and K both increase (with Na_2O<40%) while going from NBS1 to NBS2. Similar to this, NBS1 having higher R and K than NBS3, corresponded to higher density for NBS1 than NBS3. The MD estimated trend for density are in well agreement with the experimental observations[22]. Furthermore, the results show that nearly 80% oxygen atoms are dedicated to form bridging oxygen, whereas remaining 20% oxygen atoms participate as non-bridging oxygen atoms. To be noted, both R and K play in reverse direction for availability of BOs. The highest R for NBS1 correspond to lowest BO and highest K for NBS2 contribute to maximum BO for NBS2. In particular, the highest Na_2O% for NBS1 correspond to minimum number of BO available for NBS1. On the other hand, for similar content of Na_2O for NBS2 and NBS3, availability of BO is dominated by %SiO_2 in the glass. Interestingly, the number of BO_4 units in the glass matrix seem to follow the order as K i.e. NBS2>NBS1>NBS3. Additionally, the differences in short-range order of these glasses was determined in terms of minor changes in radial distribution functions and bond/angle distribution profiles. The average CN for atomic pairs is shown in Table.3.

In addition, the connectivity within structural network was noted in order Si-O-B4 > Si-O-Si > Si-O-B3 > B3-O-B4 > B4-O-B4 > B3-O-B3 for NBS1 and NBS2, whereas Si-O-B4 > Si-O-B3 > Si-O-Si > B3-O-B4 > B4-O-B4 > B3-O-B3 for NBS3. The results show that Si-O-B4 connections are favored over Si-O-Si connections. NBS3, having higher B_2O_3 content compared to NBS1 and NBS2, showed preferred connection for Si-O-B3 over Si-O-Si, on the other hand, for NBS1 and NBS2, the Si-O-Si connections were dominated over Si-O-B3. On contrary to "B[4] avoidance" rule, the present study showed abundant presence of B4-O-B4 units. The results evidence that the intermixing B3-O-B4 connections were found to be preferred over either of B3-O-B3 or B4-O-B4 connections. Also, for the simulated glasses, the B4-O-B4 linking was preferred over B3-O-B3. In particular, the relative population of these units depends on the availability of B_2O_3 and SiO_2 content[13]. For NBO, the order was Si-NBO > B3-NBO > B4-NBO, reflecting that the negatively charged BO_4- tetrahedrals usually accommodate least NBO species[12].

Furthermore, the fabrication easiness was measured in terms of glass transition temperature (Fig.6). As expected, the highest SiO_2 content in NBS2 corresponded to maximum T_g, on the other hand, the highest B_2O_3 content in NBS3 lead to lowest T_g (see Table.4). NBS1 showed the highest TEC due to the highest Na_2O content, while high B_2O_3 NBS3 was responsible for a higher TEC of NBS3 than NBS2.

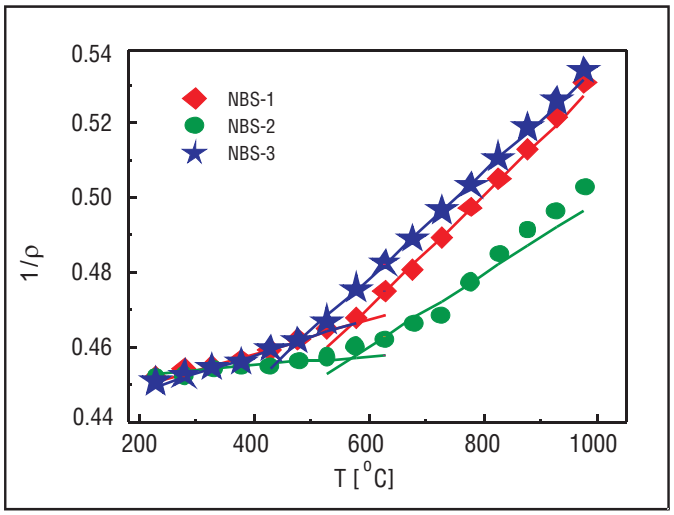

Fig.6: Inverse density vs. temperature profile for simulated NBS glasses.

Table 4. Glass Transition Temperature (T_g) and Thermal Expansion Coefficient (TEC) of simulated glasses.

	NBS1	NBS2	NBS3
T_g(^{0}C)	567.63	572.31	481.79
TEC (x 10^{-5})/^{0}C	1.13	0.73	1.05

Additionally, the mechanical strength of simulated glasses was demonstrated in terms of stress-strain relationship shown in Fig.7. The stress-strain profiles show a narrow span of plasticity before brittle fracture. The elasticity of these glasses was measured in terms of Young modulus (Y), estimated to be 40.65±1.94, 42.74±1.72, and 39.66±1.19 for NBS1, NBS2 and NBS3 respectively. The highest Y of NBS2 is owned by the highest SiO_2 and low B_2O_3 content. The modifier rich NBS1 and B_2O_3 rich NBS3 show nearly similar Y. Further, plastic nature of glass was determined in terms of yield stress, estimated to be 1.92GPa, 2.15GPa and 2.51GPa for NBS1, NBS2 and NBS3 respectively. The lowest yield stress for NBS1 is in accordance to the presence of highest Na_2O content. On the other hand, the highest yield strength for NBS3, seems to be linked with the maximum B_2O_3.

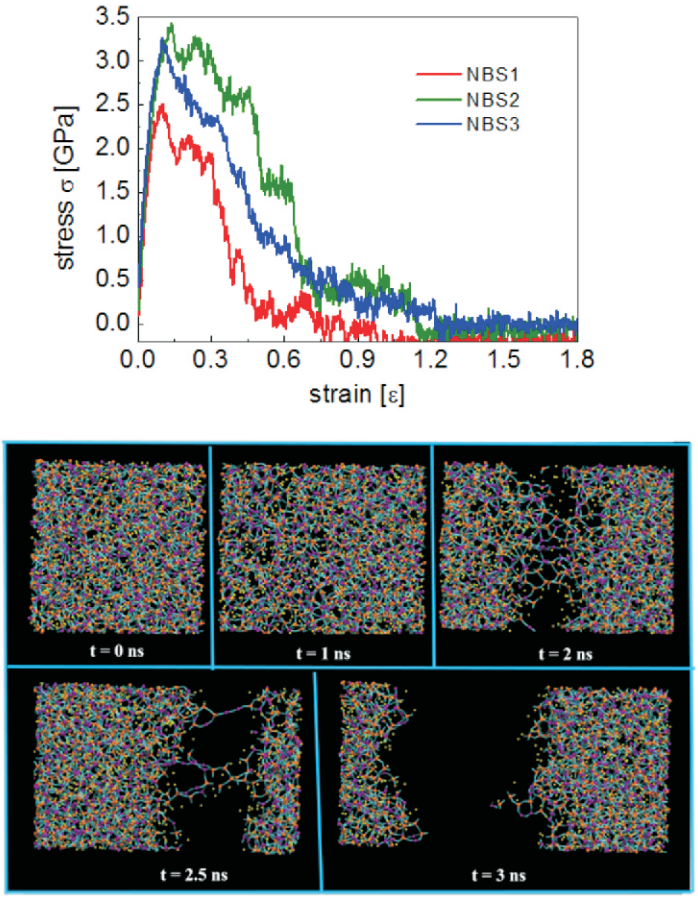

Fig.7: Stress-strain diagram and Snapshots for deformation of NBS1 glass matrix.

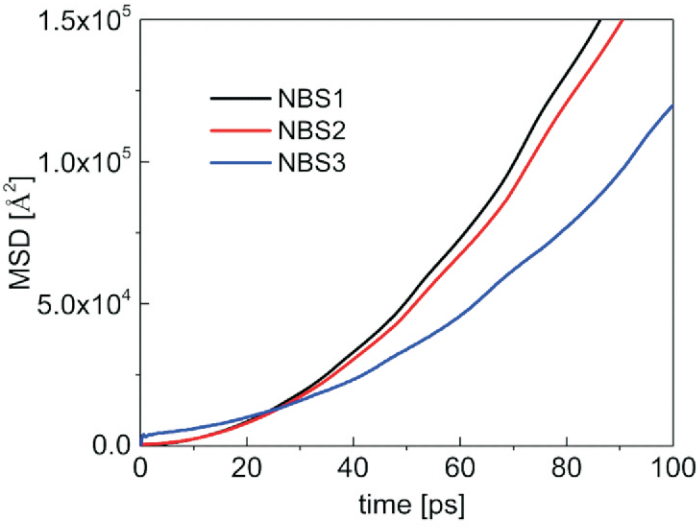

Fig.8: Mean Square Displacement (MSD) profile for sodium ions at 600K in NBS1, NBS2 and NBS3.

Table 5. Table 5. Diffusivity of sodium ions (D_{Na}) and boron atoms (D_B) [unit x10^{-7} cm^2/sec] at 600K.

Glass	D_{Na}	D_B
NBS 1	0.374 ± 0.012	0.359 ± 0.016
NBS 2	0.235 ± 0.009	0.221 ± 0.013
NBS 3	0.190 ± 0.011	0.182 ± 0.007

Furthermore, the chemical durability was determined in terms of diffusivity of component species, estimated using mean square displacement (MSD) profiles[26]. The MSD of sodium ions for the simulated glasses at 600K is shown in Fig.8 and the respective diffusion coefficients (D) are shown in Table.5. The data show that the diffusivity of sodium (Na) ions is marginally higher than the boron (B) atoms as predicted from the role of B and Na as a network former and network modifier respectively. Boron atoms, being part of network chain are not able to move freely. On the other hand, Na being network modifier, doesn't participate in network formation and so move comparatively faster than network formers. The diffusivity of both the sodium ions and boron atoms was found to be maximum for NBS1 and minimum for NBS3. The highest diffusivity of the sodium for NBS1 is linked with the presence of maximum Na_2O content for NBS1. In particular, higher the amount of network modifies, more the network connectivity is disrupted, and greater mobility of constituent atoms can be expected. However, for the similar content of Na_2O in NBS2 and NBS3, the minimum diffusivity of sodium ions and boron atoms for NBS3 is supposed to be linked with the higher B_2O_3 presence. In fact, with increasing the B_2O_3 quantity, requirement of Na^+ ions as a charge compensator to BO_4 tetrahedrals increases. It is expected that Na ions are less mobile while participating as charge compensator than their role as network modifier. As a result, the minimum diffusivity of Na^+ ions for NBS3 was observed. The presented diffusion results might be very helpful in determining the chemical durability as well as the radiation stability of simulated glass compositions as shown by Grimes and coworkers[30,31].

Effect of Cs and Sr doping in NBS glass

Cs^{137} and Sr^{90} are known as the major heat-generating isotopes in the nuclear waste, study of which is important from the perspective of chemical and mechanical strength of vitrified glass as well as for medical applications[32,33]. Here, the NBS glass was doped with 5% and 10% (by mass) Cs and Sr atoms, named as NBS- 5Cs, NBS- 5Sr, NBS- 10Cs, and NBS- 10Sr respectively. The density and T_g of these glasses is shown in Table.6.

A decrease in T_g can be noted while doping with Cs/Sr due to overall increase in alkali content which opens the network structure and reduces the melting point of glass matrix. In line to the alkali content, T_g of Sr doped glass was found to be smaller than Cs doped glass. The results in Fig.9 (a) show nearly similar number of BOs with 5% doping of Cs/Sr, however, a major difference was noticed with 10% doping of Cs/Sr. In fact, the conversion of BO to NBO depends on the charge and radius of dopant. Larger the dopant radius, more conversion of BO to NBO is expected. Secondly, the

Table 6. Density and glass transition temperature of doped sodium borosilicate glass matrixes.

Glass	Density(*exp) [g/cm^3]	T_g (*exp)[K]
NBS	2.42 (*2.4)	590 (*560)
NBS-5Cs	2.49	
NBS-10Cs	2.56 (*2.5)	545 (*532)
NBS-5Sr	2.49	
NBS-10Sr	2.55 (*2.6)	540 (*526)

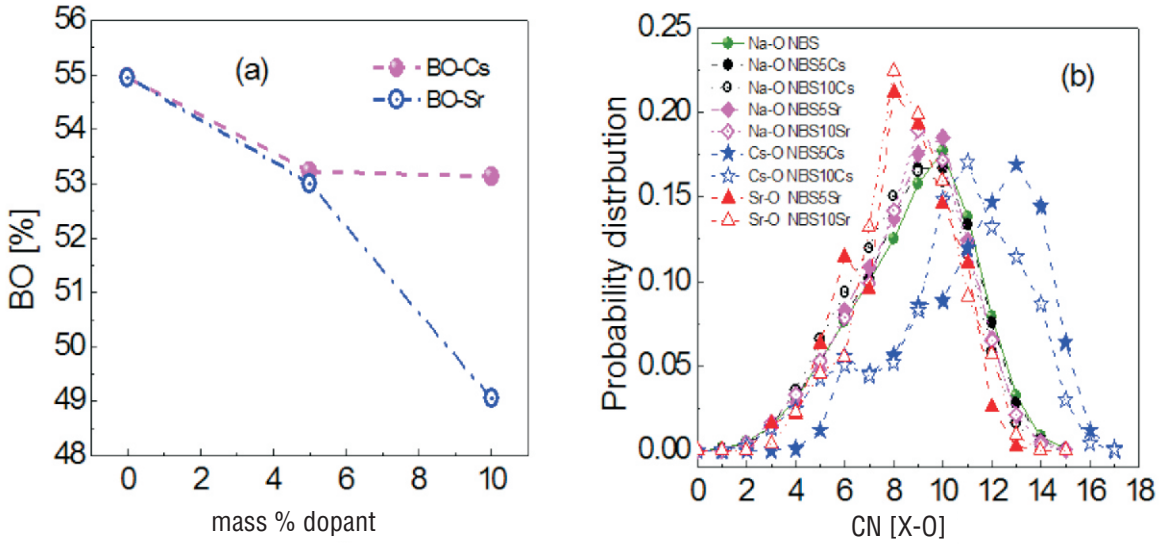

Fig.9: (a) BO and **(b)** coordination number distribution in NBS and doped NBS glass matrix.

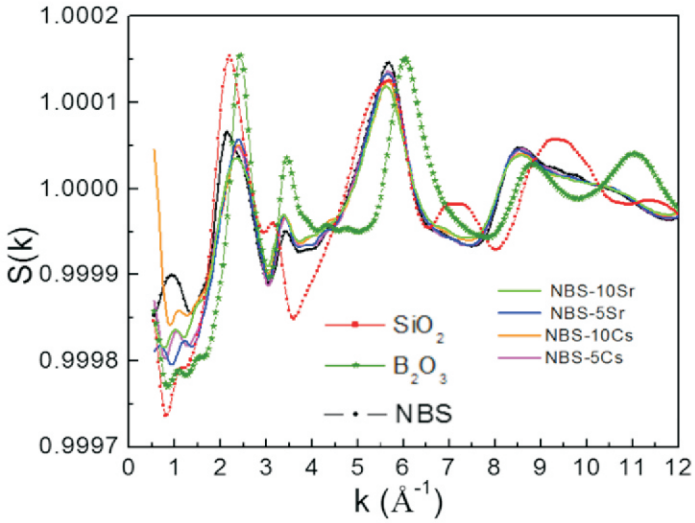

Fig.10: Structure factors for NBS glasses.

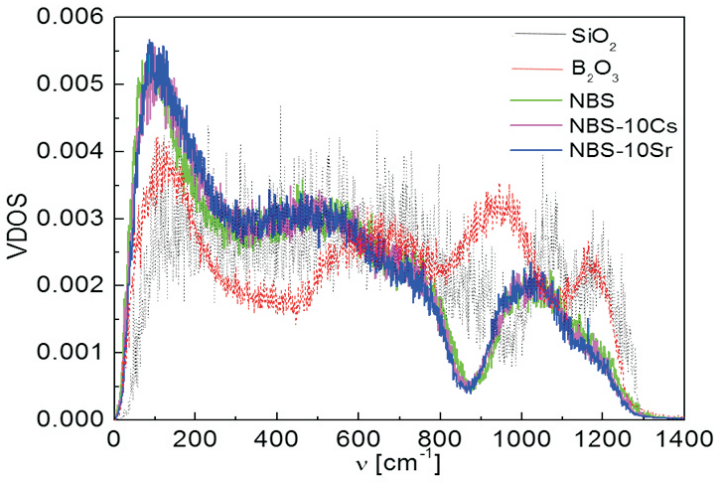

Fig.11: VDOS of NBS and doped NBS (NBS-10Cs and NBS-10Sr) and comparison with pure glass matrix of SiO_2 and B_2O_3.

dopants with higher charge will convert more BO to NBO; for example, with addition of one Cs atom only one BO will be converted to NBO; whereas presence of one Sr atom in glass matrix will convert two BOs in NBOs. Point to be noted is that the ionic radius of Cs (1.69 Å) is larger than Sr (1.33 Å), however, the charge of Cs (+1) is smaller than Sr (+2). Hereby, the ionic radius and charge on Cs and Sr interplay in the reverse direction. It seems that for lower concentration of dopants, the network connectivity is dominated by the ionic radius. However, for higher concentration of dopants (ex. 10% by mass), contribution of charges on dopants become more significant. Further, akin to other network formers, a wide spectrum for coordination number distribution was observed for Cs/Sr as shown in Fig.9 (b).

The effect of Cs and Sr doping on the intermediate range order of NBS glass was observed by structure factor (Fig.10), which showed noticeable effects in FSDP peaks of doped-NBS compared to base NBS. In particular, FSDP of NBS glass matrix were observed to split into sub-peaks while doping with Cs and Sr due to increase in alkali concentration. Another important observation was the difference in the intensity of peaks and dips, which were found to be in order of NBS>NBS-5Sr~NBS-5Cs~NBS-10Cs>NBS-10Sr, in line to availability of the BOs.

Furthermore, the characteristic VDOS (Fig.11) showed only negligible differences for Cs/Sr doped NBS compared to the bare NBS. A minor post shift at 120 cm^{-1} and pre-shift at 1100 cm^{-1} for doped NBS compared to NBS was observed, which might be associated with the weakening of Si-O_{BO}-Si network and increasing Si-O_{NBO} while doping. Also, one can notice the higher peak intensity at ~120 cm^{-1} for NBS matrix compared to pure matrix of SiO_2 and B_2O_3, and effects become more pronounced while doping of NBS with Cs and Sr, which might be associated with the increased bending and stretching motions of Si-O-Si while alkali addition.

Subsequently, the Arrhenius[34] semi-log plot of diffusivity lnD vs. 1/T was used to estimate the activation energy E_a, which were found to change while doping the NBS with Cs and Sr as shown in Table.7. In particular, the activation energy of sodium was reduced while doping or increasing the dopant concentration. Interestingly, the results show the activation energy of sodium, boron and dopants to be higher for Sr doped matrix than Cs doped matrix for doping

Table 7. Activation energy (unit eV) for migration of alkali ions and Boron atoms in NBS glass matrix and doped NBS matrix at temperature range 800K-1000K.

System	Na	Cs/Sr	B
NBS	0.942		1.065
NBS-5Cs	0.750	1.014	1.115
NBS-10Cs	0.622	0.925	0.999
NBS-5Sr	0.890	1.077	1.114
SBN10Sr	0.431	0.772	0.946

concentration of 5% by mass, however, the effects are reversed for doping concentration of 10%, where activation energy of elements was observed to be higher for Cs doped matrix than the Sr doped matrix. In real, the effects are more pronounced for Sr doping at 10%, which has been also observed while accounting of BOs in the doped NBS matrix.

Summary and Conclusion

In summary, the present article demonstrates that BKS potential model with the selected forcefield parameters can be utilized to simulate the glasses with varied composition. The results well capture the boron anomalies for varied concentration of network formers and network modifiers. Most importantly, the selected potential model and forcefield parameters not only well capture the structural distribution of glasses, but also validate the dynamic properties and characteristics vibration spectra. In addition, the validation of simulation data with the experimental observations assures the versatility of selected models for glasses of various compositions. The results establish the correlations between microscopic structure and macroscopic glass properties such as glass transition temperature, thermal expansion coefficient and mechanical integrity for glasses of varied composition. The MD results provide microscopic understanding of the glass structure and phenomena associated with the change in glass composition. The presented diffusion dynamics can be utilized to demonstrate the long-term leaching ability and radiation stability of these glasses.

The results might be very helpful in prediction of effects associated with the dopant's nature and concentration. Hereby, this article might have great academic as well technological significance for further guidance in composition selection of glass for various applications including nuclear waste immobilization.

Acknowledgement

Computer division is acknowledged for providing Anupam super computation facility.

Corresponding Author*

Sk. Musharaf Ali (musharaf@barc.gov.in)

References

[1] S. Al-Azzawi and F. Yasin, *Solar Wind Tech.*, 1985, **2**, 41-51.

[2] M.J. Plodinec, *Glass Technol-part A*, 2000, **41**, 186-192.

[3] C.P. Kaushik, *Procedia Mater. Sci.*, 2014, **7**, 16-22.

[4] H.K. Manaktala, An Assessment of Borosilicate Glass as a High-level Waste Form Nuclear Regulatory Commission Contract NRC-02-88-005 (CNWRA 92-017), San Antonio, Texas, 1992.

[5] L.-S. Du and J.F. Stebbins, *J. Phys. Chem. B* 2003, **107**, 10063-10076.

[6] S.W. Martin, A. Bhatnagar, C. Parameswar, S. Feller and J. MacKenzie, *J. Am. Ceram. Soc.*, 1995, **78**, 952-960.

[7] J.W. MacKenzie, A. Bhatnagar, D. Bain, S. Bhowmik, C. Parameswar, K. Budhwani, S.A. Feller, M.L. Royle and S.W. Martin, *J. Non-Crystal. Solids*, 1994, **177**, 269-276.

[8] A.A. Osipov, L.M. Osipova and V.E. Eremyashev, *Glass Phys. Chem.*, 2013, **39**, 105–112.

[9] Y. Yu, B. Stevensson and M. Edén, *J. Phys. Chem. C*, 2019, **123**, 25816–25832.

[10] A. Pedone, G. Malavasi, A.N. Cormack, U. Segre and M.C. Menziani, *Chem. Mater.*, 2007, **19**, 3144-3154.

[11] F. Gou, G.N. Greaves, W. Smith and R. Winter, *J. Non-Cryst. Solids.*, 2001, **293-295**, 539-546.

[12] B. Stevensson, Y. Yu and M. Eden, *Phys. Chem. Chem. Phys.*, 2018, **20**, 8192-8209.

[13] Y. Yu, B. Stevensson and M. Edén, *J. Phys. Chem. Lett.*, 2018, **9**, 6372–6376.

[14] T. Abe, *J. Am. Ceram. Soc.*, 1952, **35**, 284-299.

[15] A.C. Wright, *Phys. Chem. Glasses: Eur. J. Glass Science Technol. B*, 2010, **51**, 1-39.

[16] C.J. Phillips, *Glass Technol.*, 1964, **5**, 216-223.

[17] M.L. Williams and G.E. Scott, *Glass Technol.*, 1970, **11**, 76-79.

[18] N. Soga, *J. Non-Cryst. Solids.*, 1985, **73**, 305-313.

[19] B. Bridge, N.D. Patel and D.N. Waters, *Phys. Status Solidi A*, 1983, **77**, 655-668.

[20] S. Plimpton, *J. Comput. Phys.*, 1995, **117**, 1-19.

[21] B.W.H. v. Beest, G.J. Kramer and R.A. v. Santen, *Phys. Rev. Lett.*, 1990, **64**, 1955-1958.

[22] P. Sahu, S.M. Ali, K.T. Shenoy, S. Mohan, A. Arvind, G. Sugilal and C.P. Kaushik, *Phys. Chem. Chem. Phys.*, 2021, **23**, 14898.

[23] P. Sahu, A.A. Pente, M.D. Singh, I.A. Chowdhri, K. Sharma, M. Goswami, S.M. Ali, K.T. Shenoy and S. Mohan, *J. Phys. Chem. B*, 2019, **123**, 6290-6302.

[24] B.A. Luty and W.F.V. Gunsteren, *J. Phys. Chem.*, 1996, **100**, 2581–2587.

[25] L.-H. Kieu, J.-M. Delaye, L. Cormier and C. Stolz, *J. Non-Crystal. Solids*, 2011, **357**, 3313–3321.

[26] M.P. Allen and D.J. Tildesley, *Computer Simulation of*

Liquids, Clarendon Press, Oxford University, 2017.

[27] A.H. Verhoef and H.W. d. Hartog, *J. Non-Cryst. Solids*, 1992, **146**, 267-278.

[28] W. Kob and S. Ispas, *First-principles Simulations of Glass-formers*, 2016.

[29] L.-H. Kieu, J.-M. Delaye, L. Cormier and C. Stolz, *J. Non-Cryst. Solids*, 2011, **357**, 3313-3321.

[30] M. Bertolus, M. Freyss, B. Dorado, G. Martin, K. Hoang, S. Maillard, R. Skorek, P. Garcia, C. Valot, A. Chartier, L.V. Brutzel, P. Fossati, R.W. Grimes, D.C. Parfitt, C.L. Bishop, S.T. Murphy, M.J.D. Rushton, DragosStaicu, EugenYakub, SergiiNichenko, MatthiasKrack, FabienDevynck, RaoulNgayam-Happy, K. Govers, C.S. Deo and R.K. Behera, *J. Nucl. Mater.*, 2015, **462**, 475-495.

[31] K. Nordlund, S.J. Zinkle, A.E. Sand, F. Granberg, R.S. Averback, R.E. Stoller, T. Suzudo, L. Malerba, F. Banhart, W.J. Weber, F. Willaime, S. L. Dudarev and D. Simeone, *J. Nucl. Mater.*, 2018, **512**, 450-479.

[32] W.J. Weber, *Procedia Mater. Sci.*, 2014, **7**, 237-246.

[33] A. Vegiri, C.-P. E. Varsamis and E.I. Kamitsos, *J. Chem. Phys.*, 2005, **123**, 014508.

[34] S.A. Arrhenius, *Z. Phys. Chem.*, 1889, **4**, 96–116.